Published in final edited form as:
Biomaterials. 2011 November ; 32(31): 7785–7792. doi:10.1016/j.biomaterials.2011.07.020.

Minimally Invasive, Longitudinal Monitoring of Biomaterial-Associated Inflammation by Fluorescence Imaging

Shivaram Selvam[a,b], **Kousik Kundu**[c], **Kellie L. Templeman**[a], **Niren Murthy**[c], and **Andrés J. García**[a,b,*]

[a]Petit Institute for Bioengineering and Bioscience, 315 Ferst Drive, Atlanta, GA 30332, USA

[b]Woodruff School of Mechanical Engineering, Georgia Institute of Technology, 801 Ferst Drive, Atlanta, GA 30332, USA

[c]Wallace H. Coulter Department of Biomedical Engineering, Georgia Institute of Technology, 313 Ferst Drive, Atlanta, GA 30332, USA

Abstract

Implant-associated inflammation is a major cause for the reduced performance/lifetime and failure of numerous medical devices. Therefore, the ability to non-invasively and quantitatively monitor implant-associated inflammation is critically important. Here we show that implant-associated inflammation can be imaged via fluorescence imaging using near-infrared hydrocyanine dyes delivered either locally or intravenously in living mice. This imaging strategy allowed quantitative longitudinal monitoring of inflammation by detecting reactive oxygen species (ROS) released by inflammatory cells in response to implanted poly(ethylene terephthalate) (PET) disks or injected poly (lactic-co-glycolic acid) (PLGA) microparticles, and exhibited a strong correlation to conventional analysis of inflammation. Furthermore, modulation of inflammatory responses via controlled release of the anti-inflammatory agent dexamethasone was detected using this sensitive imaging approach. Thus, hydrocyanine-based fluorescence imaging of ROS could serve as a surrogate measure for monitoring implant-associated inflammation as well as evaluating the efficacy of therapeutic approaches to modulate host responses to implanted medical devices.

Keywords

Biocompatibility; Foreign body response; Inflammation; Free radical; Superoxide

1. Introduction

An estimated 25 million people in the U.S. alone rely on implanted medical devices [1], and the expected U.S. demand for such devices is increasing at 8% each year [2]. Although

Corresponding author: Andrés J. García, Petit Institute for Bioengineering and Bioscience, 315 Ferst Drive, 2310 IBB, Atlanta, GA 30332-0363, USA, Tel.: (404) 894-9384, Fax: (404) 385-1397, andres.garcia@me.gatech.edu.

Supplementary data

Supp. methods: Cell viability assay and characterization of PLGA-dexamethasone (PLGA-dex) microparticles.
Supp. Fig. 1: MTS cell viability assay of hydrocyanines on fibroblast (NIH 3T3) and macrophage (RAW 264.7) cultures in vitro.
Supp. Fig. 2: Characterization of PLGA-dexamethasone microparticles.

many medical devices perform adequately for years, implantation of biomaterials and medical devices elicits a dynamic host inflammatory response [3] that severely limits the integration and long-term performance of various devices, including joint prostheses, chemical biosensors, electrical leads/electrodes, therapeutic delivery systems, and tissue-engineered constructs, affecting millions of patients each year. There is therefore a compelling need for developing minimally invasive approaches to monitor and assess implant-associated inflammation, especially in clinically challenging cases involving trauma, infection, and compromised tissue beds. In addition, the ability to measure device-associated inflammation is crucial to determine when to initiate therapeutic strategies to modulate inflammation.

Current strategies to image inflammation predominantly rely on contrast agents designed for ultrasound [4] and magnetic resonance imaging [5,6]. These modalities, however, have limited potential as they can be problematic for imaging in the vicinity of devices containing metals and electromagnetic components. In addition, as the majority of these contrast agents are based on nanoparticles targeting the overexpression of cell surface receptors or the presence of inflammatory cells, the ability of these imaging agents to extravasate into the avascular fibrotic tissue surrounding the implant to reach their putative targets remains debatable due to diffusion limitations [7]. Furthermore, as most of these contrast agents rely on antibodies for targeting, they can complicate the clinical translation of these agents because of off-target effects or immune responses to these targeting antibodies. Whereas chemiluminescent agents such as luminol and its derivatives circumvent these issues and have been used for imaging implant-associated inflammation [8], the intrinsic blue spectral output of luminol (λ_{max} = 425 nm) severely limits tissue depth resolution strictly restricting its use to superficial two dimensional (2-D) visualization of only a few millimeters of tissue. Toward this end, near-infrared fluorescence (NIRF) imaging offers excellent characteristics for optical imaging [9] enabling deeper tissue penetration (up to several centimeters in various human tissues such as breast [10,11], muscle [12] and brain [13]) with reliable three-dimensional (3-D) image reconstruction [14], high sensitivity, high versatility, low autofluorescence and more importantly, substantial clinical compatibility with existing fluorescence imaging instrumentations.

We have recently developed a new family of fluorescent small molecule imaging probes, termed the hydrocyanines that possess unique physical/chemical properties for imaging ROS in vivo [15] (Fig. 1a). ROS, which comprise oxygen radicals and peroxides, have been widely implicated to play a fundamental role in the inflammatory response to implanted biomaterials [16,17]. Elevated levels of ROS, released by macrophages and neutrophils around the vicinity of an implant, act as cell signaling molecules that upregulate cytokines and other inflammatory mediators that induce inflammatory cell recruitment, foreign body giant cell formation, and fibrous encapsulation, ultimately leading to implant degradation and failure [3]. We hypothesized that the levels of ROS are a reliable indicator of the severity of inflammation and hence could serve as an excellent diagnostic marker for monitoring inflammation near the vicinity of an implanted device. Herein we describe a new minimally invasive approach for real-time fluorescence imaging of implant-associated inflammation by detecting ROS released around the vicinity of an implant (Fig. 1b, **left panel**) and longitudinally monitoring the effects of anti-inflammatory agents delivered to treat implant-associated inflammation (Fig. 1b, **right panel**) using NIRF ROS sensors. This fluorescence imaging modality represents a practical system with considerable clinical translational capability for the evaluation/diagnosis of device-associated inflammation and may enhance the development of effective therapeutic regimens to improve device biocompatibility and performance.

2. Materials and methods

2.1. Preparation of Hydrocyanines

The hydrocyanines were synthesized from cyanine dyes Cy5 (Sigma), Cy7 (Sigma), and ICG (Acros Organics) by reduction with sodium borohydride as described previously [15]. Briefly, 2 mg of dye was dissolved in 4 ml methanol (Sigma) and was reduced by adding 2 – 3 mg of sodium borohydride (Aldrich). The reaction mixture was then stirred for 5 min and the solvent was removed under reduced pressure. The resulting solid was nitrogen capped and was either used immediately or stored overnight at −20 °C. For H-Cy7, the resulting solid was further dissolved in diethyl ether and was filtered to remove solid precipitates. The solvent was removed again under reduced pressure and the reduced dye thus obtained was either used immediately without further purification or stored overnight at −20 °C.

2.2. PET implantation and ROS bioimaging in mice

Sterile, endotoxin-free PET disks (8 mm diameter) were implanted subcutaneously following IACUC-approved procedures in 6–8 wk old male BALB/c mice (Jackson Laboratories) anesthetized by isofluorane. A single 1-cm incision was made on the dorsum proximal to the spine, and a subcutaneous pocket laterally spanning the dorsum was created. Sterile disks (two per subject on either side of the spine) were implanted, and the incision was closed using sterile wound clips. Mice undergoing the same surgical procedure but receiving no biomaterial implants were used as sham controls to account for surgery-associated trauma/inflammation.

For bioimaging, 30 μl of hydro-indocyanine green (H-ICG) at a concentration of 1 mg/ml in sterile water was injected near the vicinity of the implant. Thirty minutes after dye injection, the animal was anesthetized and the whole body of the animal was scanned in an IVIS Lumina® bioimaging system (Xenogen). Biofluorescence was integrated using Living Image® software Version 3.1 (Xenogen). ROS bioimaging was performed 30 min after dye injections immediately following surgery/implantation and 1, 4, 7 and 14 days post-surgery/implantation.

2.3. Conventional implant analysis

Mice were sacrificed at specific time points (1, 4, 7 and 14 days post-implantation) and the PET disks were carefully explanted with the surrounding tissue intact to avoid disrupting the cell-material interface. Explants were embedded in optimal cutting temperature compound (Tissue-Tek) and cryosectioned at 10 μm. Histological sections were obtained with hematoxylin and eosin (H&E) staining for nuclei (dark blue) and cytoplasm (pink). For immunohistochemical staining, fresh-frozen cryostat sections were incubated in 100 μM hydro-Cy5 (H-Cy5) for 45 min at 37°C to stain for intracellular ROS. Following incubations in H-Cy5, sections were fixed with 4% paraformaldehyde and were stained with primary rat monoclonal antibodies (Abcam) against the macrophage marker, CD68 or neutrophil marker, NIMP-R14. AlexaFluor 488-conjugated goat anti-mouse specific antibody (Invitrogen) was used as a secondary antibody. The sections were mounted with antifade mounting media containing 4′,6-diamidino-2-phenylindole (DAPI, Vector Labs) and imaged under a Nikon C1 imaging system. Five-six fields per sample were acquired and ImagePro software (Media Cybernetics) was used to count the fluorescent-labeled cells.

2.4. Preparation of PLGA-dexamethasone (PLGA-dex) microparticles

Dexamethasone (Sigma) loaded or blank PLGA (RESOMER® RG 503 H, Mw 24,000–38,000, Aldrich) microparticles were prepared using a solvent evaporation method as described previously [18]. Briefly, 0.5 g PLGA was dissolved in 2 ml methylene chloride (Sigma). For dexamethasone loaded microspheres, 50 mg of dexamethasone was dispersed

in this solution using a homogenizer (PowerGen 700D, Fisher Scientific) at 9500 rpm for 2 min. This organic phase was emulsified in 10 ml of a 1% (w/v) polyvinyl alcohol (PVA, average MW 30–70 kDa, Aldrich) solution and homogenized at 10,000 rpm for 3 min. The resultant emulsion was poured into 300 ml of a 0.1% (w/v) PVA solution and stirred at 600 rpm for 3 h protected from light inside a laminar flow hood. The hardened microspheres were washed three times with de-ionized water and were collected by centrifugation at 7500 rpm for 15 min at 15 °C. The prepared microspheres were then freeze-dried under vacuum overnight and stored at −20 °C until further use.

2.5. Intramuscular injections of PLGA microparticles and longitudinal ROS bioimaging in mice

Under general anesthesia, hair from the hind legs of the animals was removed using a depilatory and cleaned with 70% isopropyl alcohol. Saline injected controls or empty PLGA particles or PLGA particles loaded with dexamethasone (5 mg in 100 μl of PBS) were then injected intramuscularly into the thigh muscle of the mice. On days 7 and 14 post-injections, 50 μl of hydro-Cy7 (H-Cy7) at a concentration of 0.5 mg/ml in saline supplemented with 10% Cremophor® EL and 10% absolute ethanol was injected into the jugular vein percutaneously. Ten - 15 minutes after intravenous dye injections, animals were scanned immediately in an IVIS Lumina® bioimaging system (Xenogen) and biofluorescence of imaging data sets was acquired and quantified using Living Image® software Version 3.1.

2.6. Statistical Analysis

Data are reported as average mean ± s.e.m. Statistical analysis was performed by two-way ANOVA using Tukey post-hoc test with $P \leq 0.05$ considered significant. For longitudinal ROS bioimaging studies, a two-way repeated measures ANOVA was used to minimize variance within subjects. Pair-wise comparisons were performed using Bonferroni post-hoc test with $P \leq 0.05$ considered significant.

3. Results

The hydrocyanines are synthesized from commercially available cyanine dyes via a one-step reduction with sodium borohydride [15]. They possess excellent stability to auto-oxidation, tunable emission wavelengths, and importantly, high selectivity and specificity as well as nanomolar sensitivity to ROS. In addition, they are small molecules that can diffuse from the injection site or vascular bed into the tissue and cells directly associated with the implanted device. These attributes render hydrocyanines ideal probes for detecting implant-associated inflammation.

We first evaluated the ability of H-ICG, a membrane impermeable NIRF ROS sensor, to image extracellular ROS associated with inflammatory responses to implanted biomaterials. Of note, ICG is a FDA-approved fluorophore that has found wide use as a non-invasive imaging agent in the human eye [19], brain [20], breast [11], liver [21], spinal cord [22], kidney [23] and cancer [11,24]. PET disks were implanted under the skin in the backs of mice. PET is used in many biomedical devices including sutures, vascular grafts, sewing cuffs for heart valves, and components for percutaneous access devices. Mice undergoing the same surgical procedure but receiving no PET implants were used as sham controls to account for surgery-associated trauma/inflammation. At prescribed times following implantation, anesthetized mice received a single local injection of H-ICG dye near the vicinity of the surgery site/implant 30 min prior to imaging via an IVIS fluorescence imaging system (Fig. 2a). Mice receiving biomaterial implants exhibited significant increases in fluorescence signal over time ($P < 0.01$), whereas the sham control showed no time-dependent differences (Fig. 2b). Importantly, the implant group displayed 2.5-fold

higher signal compared to the sham group at days 7 and 14 post-implantation. No differences in fluorescence signal were observed between implant and sham groups at the early time points. Furthermore, control mice which only received local dye injections but no surgery demonstrated significantly lower (2-fold) fluorescence signal compared to sham controls at all time points. These results demonstrate that ROS dyes injected locally can detect ROS activity associated with biomaterial-induced inflammation with no cellular toxicity (Supp. Fig. 1).

We next examined whether multiple, sequential doses of ROS dyes could be used to track ROS activity over time in the same animal. This experiment is critical to establish the potential of these dyes as minimally invasive sensors for continuously monitoring inflammation. As shown in Fig. 2c, no differences in fluorescence signal were observed between mice receiving a dye injection only once (30 min prior to imaging) or mice receiving an injection at multiple time points 30 min prior to imaging. To exclude the possibility that the fluorescence signal observed was residual fluorescence from sensors delivered at previous time points, mice in the multiple dosing group were scanned before each imaging session. These results showed that fluorescence signals decreased to near or comparable background imaging levels before the start of an active imaging session, demonstrating dye clearance. This result confirmed that the observed fluorescence values were due to the ROS sensor delivered 30 min before the current imaging session rather than residual fluorescence from previous dye injections.

Following imaging, mice were sacrificed and the PET disks were retrieved along with implant-associated tissues and analyzed for conventional measures of inflammation to correlate the ROS signal with implant-related inflammation. Histological analysis showed the formation of a collagenous fibrous capsule around the implants of increasing thickness with implantation time (Fig. 3a), a hallmark of chronic inflammation to biomaterials. We measured the fibrous capsule thickness of the explants (Fig. 3b) and correlated them with the corresponding ROS fluorescence signals. Remarkably, fibrous capsule thickness correlated strongly with the ROS fluorescence signal ($\rho \sim 0.97$) (Fig. 3c). This result indicates that ROS imaging can be used as a minimally invasive surrogate measure of biomaterial-associated fibrous capsule formation.

Using immunohistochemistry, we analyzed macrophage (CD68+) and neutrophil (NIMP-R14+) recruitment to the implant (Fig. 4). In addition, we co-stained for ROS activity using hydro-Cy5 (H-Cy5) as previously described [25] (Fig. 4a). We observed a massive influx of inflammatory cells (>80% of all cells; 45% neutrophils, 35% macrophages) to the vicinity of the implant at the acute stages of implantation (day 1) (Fig. 4b). Over time, the number of neutrophils steadily decreased (<20% by day 14) whereas the number of macrophages remained constant around 30% of the total number of cells (Fig. 4b). This time-dependent cellular profile is consistent with previous analyses [3]. Importantly, co-staining analysis for inflammatory cell markers and ROS activity demonstrated that neutrophils and macrophages are primarily responsible for the ROS activity associated with the implant (Fig. 4c). At day 1, over 90% of the ROS activity co-localized with neutrophils and macrophages (Fig. 4c). By day 14, macrophages co-localized with >60% of ROS activity while neutrophils had lower (20%) co-localization with ROS activity (Fig. 4c). This constant expression of ROS activity by macrophages and decrease in neutrophil activity are in excellent agreement with literature [3]. Taken together, these results demonstrate that minimally-invasive ROS imaging provides a reliable marker of biomaterial-associated inflammation and can be correlated to standard, end-point/destructive analyses of inflammation.

We next examined whether our imaging strategy could detect attenuation in inflammatory responses in response to delivery of anti-inflammatory agents from PLGA microparticles.

PLGA is a FDA-approved degradable polymer used in sutures, orthopedic devices, and drug delivery matrices. PLGA microparticles loaded with or without the anti-inflammatory drug dexamethasone (dex) were prepared using standard methods. These biomaterial particles provide for controlled release of dex (Supp. Fig. 2). Empty PLGA microparticles or PLGA microparticles loaded with dex were injected into the thigh muscle of mice. Mice receiving saline were treated as controls (Fig. 5a).

To image inflammation, we chose H-Cy7, a membrane permeable intracellular ROS sensor, for intravenous (i.v.) delivery at days 7 and 14 post-microparticle injection (Fig. 5a). The rationale for choosing H-Cy7 is that upon oxidation with intracellular ROS, H-Cy7 becomes a charged and membrane impermeable molecule thereby accumulating within cells that overproduce ROS. We hypothesized that this unique property would allow for a reduced working concentration and injection volume of H-Cy7 enabling a high signal to noise ratio. Animals were imaged in an IVIS imaging system 10–15 min after intravenous injections (Fig. 5a). Empty PLGA microparticles generated strong ROS signals that increased over time and were significantly higher than the saline-only controls (Fig. 5b,c). This strong ROS signal is expected because PLGA microparticles generate significant inflammation. Importantly, the ROS signal was localized to the area where the microparticles were injected. This result demonstrates that intravenously delivered ROS sensors can detect local inflammatory responses to biomaterials. Furthermore, the ROS signal associated with PLGA microparticles releasing dex was significantly lower than the signal for empty microparticles (Fig. 5b,c), showing that the ROS sensors can be used to monitor the effects of therapeutic anti-inflammatory agents.

We next performed histological analysis on the explanted thigh muscle of mice. We observed significantly higher number of inflammatory cells around empty PLGA microparticles compared to PLGA microparticles releasing dex (Fig. 5d). This result was further confirmed by immunohistochemical staining for CD68 which showed significantly higher numbers of macrophages around empty PLGA microparticles than around PLGA microparticles releasing dex (Fig. 5e). Consistent with our previous observations, these results demonstrate that the ROS signal correlates with conventional markers of implant-associated inflammation.

4. Discussion

The development of NIR flurophores and nanoparticles has led to significant advances in non-invasive imaging of key biological processes ranging from molecular function to inflammatory pathological disease states. Notably, in vivo NIRF imaging has been extensively employed to investigate the role of inflammation in atherosclerosis [26], asthma [27], arthritis [28], chronic kidney disease [29], muscular dystrophy [30], intestinal injury [31] and inflammatory plasma leakage [32]. Activated macrophages, the major effector cell type that predominate across all these inflammatory disease states, upregulate the release of a broad spectrum of inflammatory mediators including ROS, cytokines, chemokines and proinflammatory signaling molecules that promote disease progression. In biomedical applications, implanted biomaterials have shown to induce inflammatory cells to produce ROS throughout the lifetime of an implant often leading to implant failure [3]. Evidently, ROS released by stimulated macrophages present an attractive target for developing de novo molecular imaging strategies to define and understand the inflammatory processes and to devise effective diagnostic and therapeutic approaches to treat these inflammatory conditions. In this study, we have exploited the increased levels of ROS present near the vicinity of an implant to develop a minimally invasive NIRF imaging modality to visualize implant-associated inflammation using novel fluorescent ROS sensors termed the hydrocyanines.

The hydrocyanines are fluorescent probes in the NIR spectral region (600 nm – 900 nm) that can detect ROS in living cells and tissues in vivo [15]. In their reduced state, they are weakly fluorescent because of their disrupted π conjugation; however, oxidation with ROS regenerates their extended π conjugation dramatically increasing their fluorescence intensity [15]. Although fluorescent probes such as dihydroethidium, dihydrorhodamine, or sulphonate ester-based dyes have been used for detecting ROS, their spontaneous auto-oxidation, rapid photobleaching, high toxicity, low emission wavelengths, and multiple reaction products with ROS severely limit their applications for in vivo imaging [33,34]. Recently, luminol-mediated chemiluminescence imaging has shown promise for imaging implant-associated inflammation in vivo [8]. While useful, luminol reacts with many ROS products and oxidizing agents released during phagocytic oxidative burst [8,35] and hence does not possess the required specificity and selectivity for detecting specific ROS levels as the hydrocyanines [15]. Furthermore, chemiluminescence imaging has limited clinical applicability as it is characterized by low sensitivity in the visible region, limited availability of luminescent probes, reduced tissue penetration depth at shorter wavelengths that restricts it to 2-D imaging, and presents a significant challenge for 3-D image reconstruction.

By contrast, numerous NIRF agents are widely in use for various analytical and diagnostic applications [36]. Furthermore, the applicability of these NIRF agents as targeted molecular probes for various imaging modalities is quite promising. For example, the IRDye® 800CW imaging agents from LI-COR® are moving towards FDA approval for use in various clinical applications including tumor targeting, angiography and image-guided surgery. Similarly, NIRF probes for catheter-based imaging of high-risk plaques in coronary-sized arteries [26,37] are gaining traction for evaluation in human clinical trials. In addition, comprehensive 3-D visualizations of tumor xenografts [14] and bone remodeling [38] have already been demonstrated in living mice using NIR probes via fluorescence lifetime tomography and fluorescence molecular tomography. Although the 3-D spatial resolution in fluorescence imaging is currently limited, this shortcoming may be overcome by combining it with high resolution anatomical imaging modalities such as magnetic resonance imaging and X-ray computed tomography through multimodal imaging [39,40]. These advancements are significant and highlight the myriad possibilities that hydrocyanine-based fluorescence imaging could offer for imaging ROS implicated in the development and progression of inflammatory pathologies in various disease states.

5. Conclusions

Implant-associated inflammation can be readily imaged via fluorescence imaging using NIR hydrocyanine dyes delivered either locally or intravenously in living mice. The ability to deliver these NIR small-molecule probes intravenously to monitor local implant-related inflammation is a critical feature for practical imaging in deeper tissues and overcomes limitations associated with antibody-functionalized nanoparticles and chemiluminescence substrates. This imaging strategy provides for quantitative, longitudinal monitoring of inflammation by detecting ROS released by inflammatory cells in response to implanted medically-relevant polymeric bulk discs and microparticles. Importantly, the ROS signal intensity serves as a surrogate measure of inflammation, strongly correlating to conventional analysis of inflammation such as neutrophil and macrophage recruitment and fibrous capsule thickness. Furthermore, the hydrocyanines can be used to evaluate the efficacy of therapeutic approaches to modulate host responses to implanted medical devices.

Supplementary Material

Refer to Web version on PubMed Central for supplementary material.

Acknowledgments

This work was supported by Georgia Tech/Emory Center (GTEC) for the Engineering of Living Tissues and the Atlanta Clinical and Translational Science Institute (ACTSI) supported in part by PHS Grant UL1 RR025008 from the Clinical and Translational Science Award program, Federal funds from the National Heart, Lung, and Blood Institute, National Institutes of Health (1R01HL096796-01 to N.M.), Department of Health and Human Services, under Contract No. HHSN268201000043C, and National Center for Research Resources.

References

1. Hanna, KE. Institute of Medicine (U.S.). Innovation and invention in medical devices : workshop summary. Washington, D.C: National Academy Press; 2001. Roundtable on Research and Development of Drugs B, and Medical Devices.
2. The Freedonia Group. Cleveland, USA: Freedonia; 2010. Implantable Medical Devices to 2014 - Demand and Sales Forecasts, Market Share, Market Size, Market Leaders. Online. Available from URL: http://www.freedoniagroup.com/Implantable-Medical-Devices.html
3. Anderson JM, Rodriguez A, Chang DT. Foreign body reaction to biomaterials. Semin Immunol. 2008; 20(2):86–100. [PubMed: 18162407]
4. Kaufmann BA, Sanders JM, Davis C, Xie A, Aldred P, Sarembock IJ, et al. Molecular imaging of inflammation in atherosclerosis with targeted ultrasound detection of vascular cell adhesion molecule-1. Circulation. 2007; 116(3):276–284. [PubMed: 17592078]
5. Boutry S, Burtea C, Laurent S, Toubeau G, Vander Elst L, Muller RN. Magnetic resonance imaging of inflammation with a specific selectin-targeted contrast agent. Magn Reson Med. 2005; 53(4): 800–807. [PubMed: 15799062]
6. Breckwoldt MO, Chen JW, Stangenberg L, Aikawa E, Rodriguez E, Qiu S, et al. Tracking the inflammatory response in stroke in vivo by sensing the enzyme myeloperoxidase. Proc Natl Acad Sci USA. 2008; 105(47):18584–18589. [PubMed: 19011099]
7. von zur Muhlen C, Fink-Petri A, Salaklang J, Paul D, Neudorfer I, Berti V, et al. Imaging monocytes with iron oxide nanoparticles targeted towards the monocyte integrin MAC-1 (CD11b/CD18) does not result in improved atherosclerotic plaque detection by in vivo MRI. Contrast Media Mol Imaging. 2010; 5(5):268–275. [PubMed: 20973112]
8. Liu WF, Ma M, Bratlie KM, Dang TT, Langer R, Anderson DG. Real-time in vivo detection of biomaterial-induced reactive oxygen species. Biomaterials. 2011; 32(7):1796–1801. [PubMed: 21146868]
9. Hilderbrand SA, Weissleder R. Near-infrared fluorescence: application to in vivo molecular imaging. Curr Opin Chem Biol. 2010; 14(1):71–79. [PubMed: 19879798]
10. Fang Q, Carp SA, Selb J, Boverman G, Zhang Q, Kopans DB, et al. Combined optical imaging and mammography of the healthy breast: optical contrast derived from breast structure and compression. IEEE Trans Med Imaging. 2009; 28(1):30–42. [PubMed: 19116186]
11. Mieog JS, Troyan SL, Hutteman M, Donohoe KJ, van der Vorst JR, Stockdale A, et al. Toward Optimization of Imaging System and Lymphatic Tracer for Near-Infrared Fluorescent Sentinel Lymph Node Mapping in Breast Cancer. Ann Surg Oncol. 2011
12. Geraskin D, Boeth H, Kohl-Bareis M. Optical measurement of adipose tissue thickness and comparison with ultrasound, magnetic resonance imging, and callipers. J Biomed Opt. 2009; 14(4) 044017.
13. Hoge RD, Franceschini MA, Covolan RJ, Huppert T, Mandeville JB, Boas DA. Simultaneous recording of task-induced changes in blood oxygenation, volume, and flow using diffuse optical imaging and arterial spin-labeling MRI. Neuroimage. 2005; 25(3):701–707. [PubMed: 15808971]
14. Bloch S, Lesage F, McIntosh L, Gandjbakhche A, Liang K, Achilefu S. Whole-body fluorescence lifetime imaging of a tumor-targeted near-infrared molecular probe in mice. J Biomed Opt. 2005; 10(5) 054003.
15. Kundu K, Knight SF, Willett N, Lee S, Taylor WR, Murthy N. Hydrocyanines: a class of fluorescent sensors that can image reactive oxygen species in cell culture, tissue, and in vivo. Angew Chem Int Ed Engl. 2009; 48(2):299–303. [PubMed: 19065548]

16. Hooper KA, Nickolas TL, Yurkow EJ, Kohn J, Laskin DL. Characterization of the inflammatory response to biomaterials using a rodent air pouch model. J Biomed Mater Res. 2000; 50(3):365–374. [PubMed: 10737878]

17. Tsaryk R, Kalbacova M, Hempel U, Scharnweber D, Unger RE, Dieter P, et al. Response of human endothelial cells to oxidative stress on Ti6Al4V alloy. Biomaterials. 2007; 28(5):806–813. [PubMed: 17049373]

18. Bhardwaj U, Sura R, Papadimitrakopoulos F, Burgess DJ. PLGA/PVA hydrogel composites for long-term inflammation control following s.c. implantation. Int J Pharm. 2010; 384(1–2):78–86. [PubMed: 19800956]

19. Owens SL. Indocyanine green angiography. Br J Ophthalmol. 1996; 80(3):263–266. [PubMed: 8703866]

20. Keller E, Froehlich J, Muroi C, Sikorski C, Muser M. Neuromonitoring in intensive care: a new brain tissue probe for combined monitoring of intracranial pressure (ICP) cerebral blood flow (CBF) and oxygenation. Acta Neurochir Suppl. 2011; 110(Pt 2):217–220. [PubMed: 21125474]

21. Mizuno S, Isaji S. Indocyanine green (ICG) fluorescence imaging-guided cholangiography for donor hepatectomy in living donor liver transplantation. Am J Transplant. 2010; 10(12):2725–2726. [PubMed: 21062417]

22. Murakami T, Koyanagi I, Kaneko T, Iihoshi S, Houkin K. Intraoperative indocyanine green videoangiography for spinal vascular lesions: case report. Neurosurgery. 2011; 68(1 Suppl Operative):241–245. [PubMed: 21206310]

23. Sawada T, Solly M, Kita J, Shimoda M, Kubota K. An alternative tool for intraoperative assessment of renal vasculature after revascularization of a transplanted kidney. Am J Surg. 2010; 199(6):e69–e71. [PubMed: 20409513]

24. Schaafsma BE, Mieog JS, Hutteman M, van der Vorst JR, Kuppen PJ, Lowik CW, et al. The clinical use of indocyanine green as a near-infrared fluorescent contrast agent for image-guided oncologic surgery. J Surg Oncol. 2011

25. Lin PW, Myers LE, Ray L, Song SC, Nasr TR, Berardinelli AJ, et al. Lactobacillus rhamnosus blocks inflammatory signaling in vivo via reactive oxygen species generation. Free Radic Biol Med. 2009; 47(8):1205–1211. [PubMed: 19660542]

26. Calfon MA, Vinegoni C, Ntziachristos V, Jaffer FA. Intravascular near-infrared fluorescence molecular imaging of atherosclerosis: toward coronary arterial visualization of biologically high-risk plaques. J Biomed Opt. 2010; 15(1) 011107.

27. Korideck H, Peterson JD. Noninvasive quantitative tomography of the therapeutic response to dexamethasone in ovalbumin-induced murine asthma. J Pharmacol Exp Ther. 2009; 329(3):882–889. [PubMed: 19293392]

28. Fischer T, Gemeinhardt I, Wagner S, Stieglitz DV, Schnorr J, Hermann KG, et al. Assessment of unspecific near-infrared dyes in laser-induced fluorescence imaging of experimental arthritis. Acad Radiol. 2006; 13(1):4–13. [PubMed: 16399028]

29. Nakamura K, Tabata Y. A new fluorescent imaging of renal inflammation with RCP. J Control Release. 2010; 148(3):351–358. [PubMed: 20849894]

30. Baudy AR, Sali A, Jordan S, Kesari A, Johnston HK, Hoffman EP, et al. Non-invasive optical imaging of muscle pathology in mdx mice using cathepsin caged near-infrared imaging. Mol Imaging Biol. 2011; 13(3):462–470. [PubMed: 20661652]

31. Costantini TW, Eliceiri BP, Peterson CY, Loomis WH, Putnam JG, Baird A, et al. Quantitative assessment of intestinal injury using a novel in vivo, near-infrared imaging technique. Mol Imaging. 2010; 9(1):30–39. [PubMed: 20128996]

32. Kim MH, Curry FR, Simon SI. Dynamics of neutrophil extravasation and vascular permeability are uncoupled during aseptic cutaneous wounding. Am J Physiol Cell Physiol. 2009; 296(4):C848–C856. [PubMed: 19176758]

33. Zielonka J, Vasquez-Vivar J, Kalyanaraman B. Detection of 2-hydroxyethidium in cellular systems: a unique marker product of superoxide and hydroethidine. Nat Protoc. 2008; 3(1):8–21. [PubMed: 18193017]

34. Zhao H, Joseph J, Fales HM, Sokoloski EA, Levine RL, Vasquez-Vivar J, et al. Detection and characterization of the product of hydroethidine and intracellular superoxide by HPLC and

limitations of fluorescence. Proc Natl Acad Sci USA. 2005; 102(16):5727–5732. [PubMed: 15824309]

35. Gross S, Gammon ST, Moss BL, Rauch D, Harding J, Heinecke JW, et al. Bioluminescence imaging of myeloperoxidase activity in vivo. Nat Med. 2009; 15(4):455–461. [PubMed: 19305414]
36. Escobedo JO, Rusin O, Lim S, Strongin RM. NIR dyes for bioimaging applications. Curr Opin Chem Biol. 2010; 14(1):64–70. [PubMed: 19926332]
37. Zhu B, Jaffer FA, Ntziachristos V, Weissleder R. Development of a near infrared fluorescence catheter: operating characterisitics and feasibility for atherosclerotic plaque detection. J. Phys. D: Appl. Phys. 2005; 38(15):2701–2707.
38. Zilberman Y, Kallai I, Gafni Y, Pelled G, Kossodo S, Yared W, et al. Fluorescence molecular tomography enables in vivo visualization and quantification of nonunion fracture repair induced by genetically engineered mesenchymal stem cells. J Orthop Res. 2008; 26(4):522–530. [PubMed: 17985393]
39. Talanov VS, Regino CA, Kobayashi H, Bernardo M, Choyke PL, Brechbiel MW. Dendrimer-based nanoprobe for dual modality magnetic resonance and fluorescence imaging. Nano Lett. 2006; 6(7):1459–1463. [PubMed: 16834429]
40. Guo X, Liu X, Wang X, Tian F, Liu F, Zhang B, et al. A combined fluorescence and microcomputed tomography system for small animal imaging. IEEE Trans Biomed Eng. 2010; 57(12):2876–2883. [PubMed: 20833597]

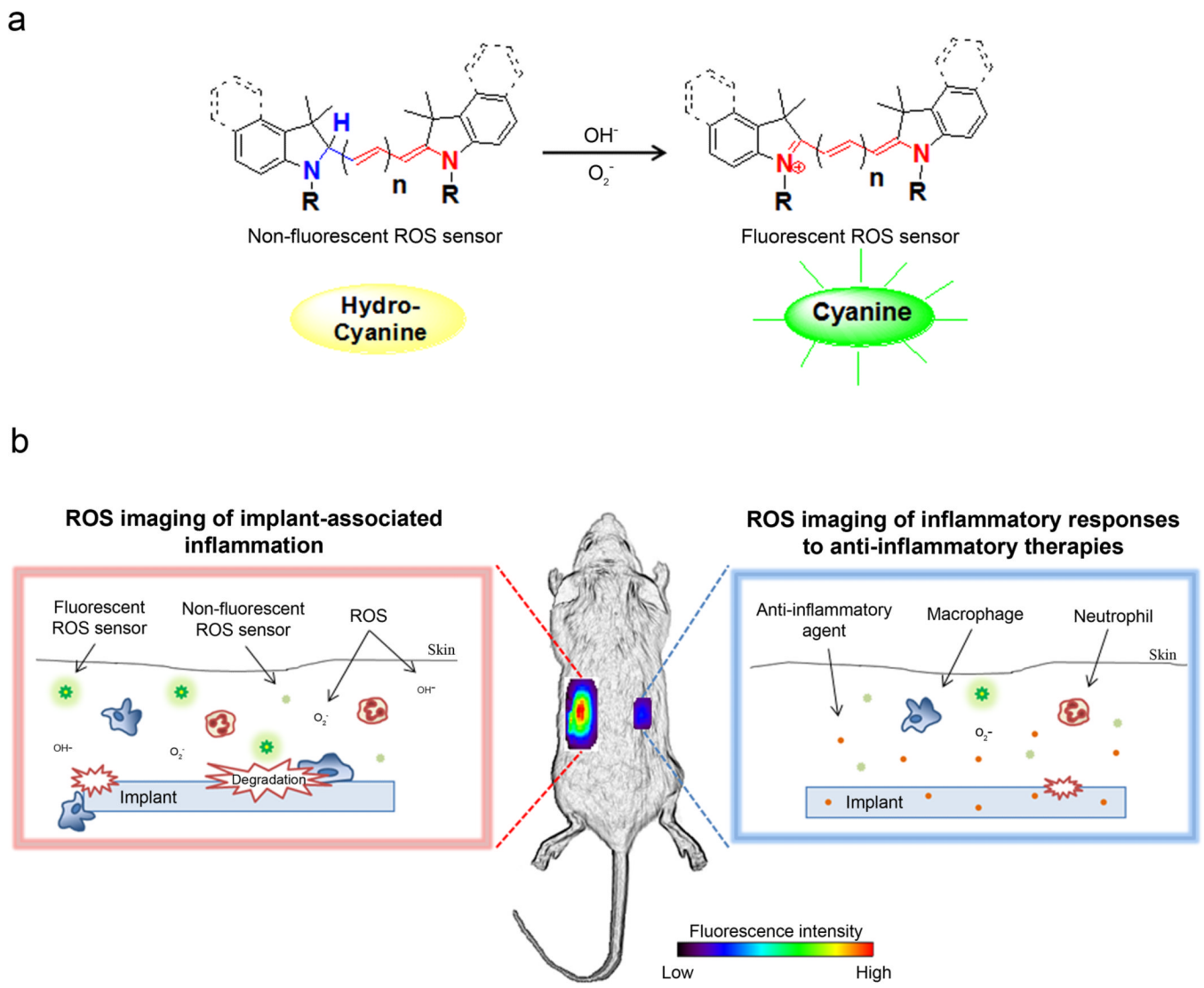

Fig. 1.

Near-infrared fluorescence imaging of ROS as a surrogate measure for monitoring implant-associated inflammation. (a) Hydrocyanine ROS sensors are synthesized from cyanine dyes via one-step reduction with sodium borohydride. Reaction with superoxide or hydroxyl radical oxidizes the hydrocyanines into fluorescent cyanine dyes, which can be detected in vivo by fluorescent imaging. (b) ROS released by inflammatory cells in response to implanted biomaterials can be detected and monitored using NIR hydrocyanine ROS sensors delivered either locally or intravenously in living mice (left panel). Attenuation of inflammatory responses in response to controlled release of anti-inflammatory agents can also be detected using this sensitive imaging approach (right panel).

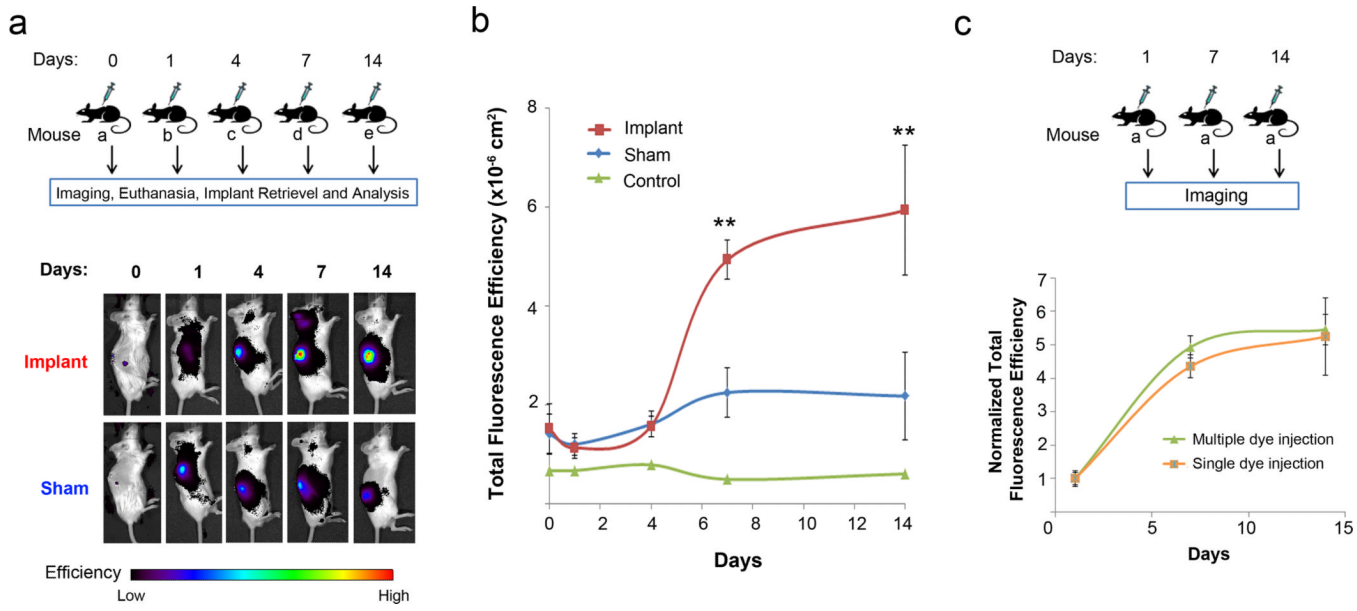

Fig. 2.

ROS imaging of implant-associated inflammation after subcutaneous administration of H-ICG. **(a)** Schematic showing the experimental study design of animals that received only a single dye injection at any given time point. Thirty minutes after the dye injection the whole body of the animal was scanned in an IVIS® imaging system and the biofluorescence was integrated. Shown below is the representative image of the bioimaging data obtained from animals in the sham and implant groups tracked for a period of 14 days. **(b)** Quantification of ROS fluorescence data from mice in the single dye injection group with dye-only injected control, sham and implant groups (± s.e.m.) (**$P < 0.01$ between sham and implant, $n \geq 5$ mice/time point for sham and implant groups). **(c)** Schematic showing the experimental design for longitudinal monitoring of implant-associated inflammation in mice that received dye injections at multiple time points including, 1, 7, and 14 days post-implantation. Shown below is the normalized ROS fluorescence data (± s.e.m.) from mice that received only a single dye injection at any given time point ($n \geq 3$ mice/time point) to animals that received sequential dye injections at multiple time points ($n = 3$ mice). No significant differences were observed between the two groups.

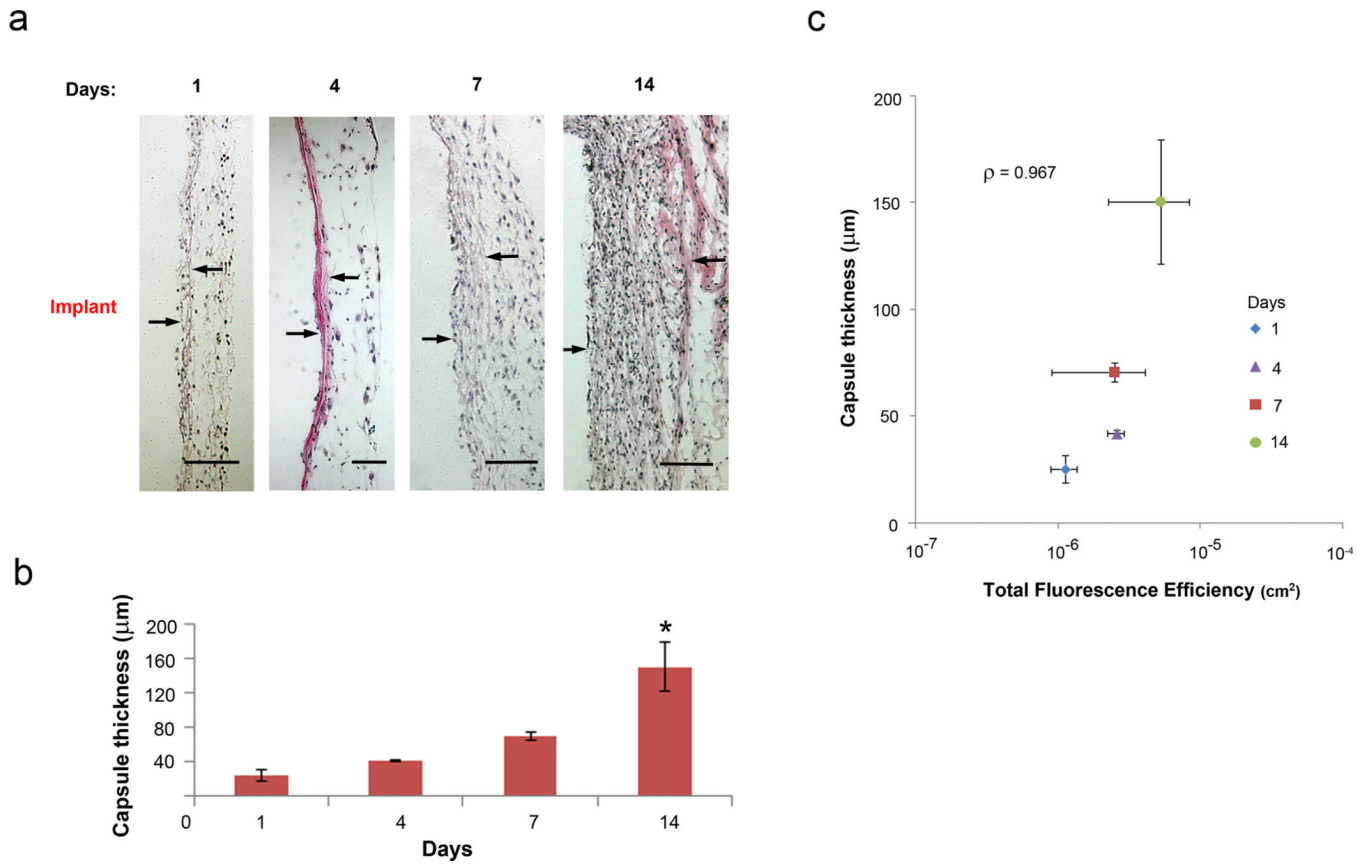

Fig. 3.

Histological analysis of implant-associated inflammation at the tissue-implant interface. **(a)** Representative sections of tissue response showing fibrous capsules (arrows) to subcutaneously implanted PET disks tracked for a period of 14 days. Scale bars, 100 μm. **(b)** Measurement of fibrous capsule thickness associated with PET implants (± s.e.m.) increased with time (*$P < 0.05$, $n = 3$ mice/time point). **(c)** Correlation of fibrous capsule thickness to corresponding ROS fluorescence values (± s.e.m.), ($n = 3$ mice/time point). Fibrous capsule thickness correlated strongly with the ROS fluorescence signal with Pearson correlation coefficient, $\rho \sim 0.97$.

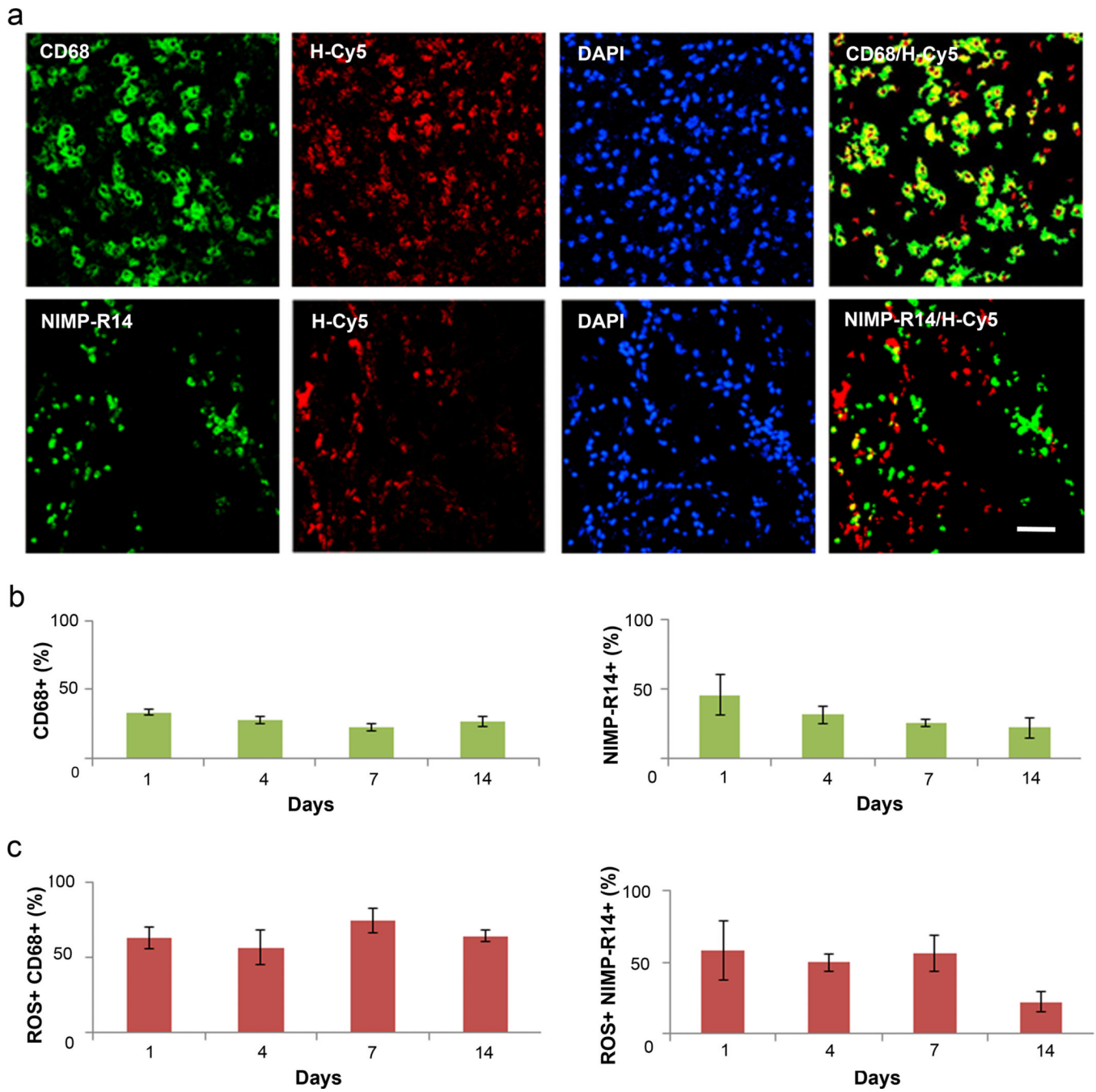

Fig. 4.

Immunohistochemical staining for macrophages and neutrophils in implant-associated inflammation. **(a)** Representative co-localization images of macrophages (CD68+, green) and neutrophils (NIMP-R14+, green) with intracellular ROS (H-Cy5+, red) in 14-day implants. Nuclei are stained with DAPI (4',6-diamidino-2-phenylindole). Scale bar, 50 μm. **(b)** Quantification of CD68+ and NIMP-R14+ cells (± s.e.m.), (*n* = 4 mice/time point). **(c)** Quantification of ROS+ cells that stained positive for CD68 and NIMP-R14 (± s.e.m.), (*n* = 4 mice/time point).

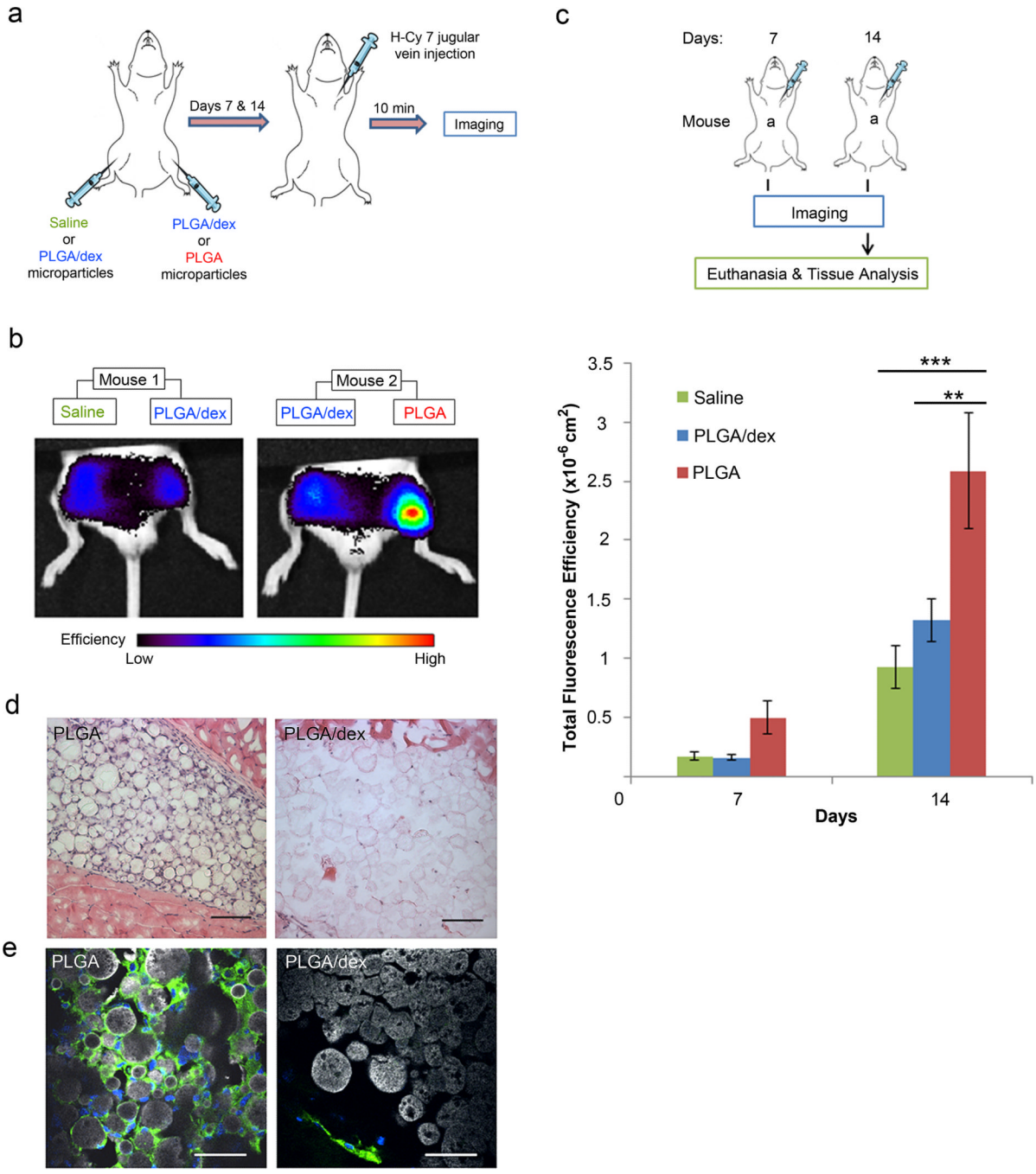

Fig. 5.

Longitudinal ROS imaging in response to controlled release of dexamethasone from PLGA microparticles after intravenous delivery of H-Cy7. **(a)** Schematic showing the experimental study design for animals receiving microparticle injections. Empty PLGA microparticles, PLGA microparticles loaded with dexamethasone and saline controls were injected into the thigh muscle of mice. At days 7 and 14 post-microparticle injection, H-Cy7 was injected intravenously into the jugular vein. Ten min after dye injections, the whole body of the animal was scanned in an IVIS® imaging system and the biofluorescence was integrated. **(b)** Representative images of the ROS imaging data from animals showing the three different groups. **(c)** Schematic showing the experimental design and quantification of the ROS

imaging data (± s.e.m.) obtained from mice with the three different groups tracked for a period of 2 weeks (**$P < 0.01$, ***$P < 0.001$, $n \geq 5$ mice/time point). **(d)** Representative images of histological tissue sections from mice injected with empty PLGA microparticles and PLGA microparticles loaded with dexamethasone in 14-day explants. Scale bars, 100 μm. **(e)** Representative images of tissues in 14-day explants immunostained for macrophages (CD68+, green), nuclei (DAPI, blue) and microparticles (grey). Scale bars, 50 μm.